Mode-Locked Ultrashort Pulse Generation from On-Chip Normal Dispersion Microresonators

S.-W. Huang, H. Zhou, J. Yang, J. F. McMillan, A. Matsko, M. Yu, D.-L. Kwong, L. Maleki, and C. W. Wong

Phys. Rev. Lett. **114**, 053901 — Published 4 February 2015

DOI: 10.1103/PhysRevLett.114.053901

Mode-locked ultrashort pulse generation from on-chip normal dispersion microresonators

S.-W. Huang[1,2,*], H. Zhou[1], J. Yang[1,2,], J. F. McMillan[1], A. Matsko[3], M. Yu[4], D.-L. Kwong[4], L. Maleki[3], and C. W. Wong[1, 2,†]

[1] Optical Nanostructures Laboratory, Center for Integrated Science and Engineering, Solid-State Science and Engineering, and Mechanical Engineering, Columbia University, New York, 10027

[2] Mesoscopic Optics and Quantum Electronics, University of California, Los Angeles, CA 90095

[3] OEwaves Inc, Pasadena, CA 91107

[4] Institute of Microelectronics, Singapore, Singapore 117685

Abstract: We describe the generation of stable mode-locked pulse trains from on-chip normal dispersion microresonators. The excitation of hyper-parametric oscillation is facilitated by the local dispersion disruptions induced by mode interactions. The system is then driven from hyper-parametric oscillation to the mode-locked state with over 200 nm spectral width by controlled pump power and detuning. With the continuous-wave driven nonlinearity, the pulses sit on a pedestal, akin to a cavity soliton. We identify the importance of pump detuning and wavelength-dependent quality factors in stabilizing and shaping the pulse structure, to achieve a single pulse inside the cavity. We examine the mode-locking dynamics by numerically solving the master equation and provide analytic solutions under appropriate approximations.

PACS numbers: (42.65.Re) Ultrafast processes; optical pulse generation and pulse compression, (42.65.Hw) Phase conjugation; photorefractive and Kerr effects, (42.55.Sa)

Microcavity and microdisk lasers, (42.65.Yj) Optical parametric oscillators and amplifiers.

Recently continuous-wave (cw) pumped monolithic microresonators emerge as promising platforms for compact optical frequency comb generation [1–11]. With anomalous group-velocity-dispersion (GVD) and self-phase modulation (SPM), optical solitons can be generated [12,13], and remarkably broad bandwidths [6] and RF-optical stability [3] have been demonstrated. Obtaining anomalous GVD broadly across arbitrary center frequencies, however, is challenging for microresonators [14]. Dispersion engineering by conformal coating [15–17] and waveguide shaping [18] are possible, but often lead to lower quality factors (*Q*s). Alternatively, frequency comb and ultrashort pulse generation from normal GVD microresonators has been theoretically predicted [19–21] and comb-like spectra from normal GVD crystalline resonators were recently measured [22,23]. Further investigation into this normal GVD architecture, especially in the time-domain and that of coherent mode-locking, will open up new fields in chip-scale oscillators, waveform generation, and ultrafast spectroscopy.

Here we report mode-locked pulse generation from on-chip normal dispersion microresonators. The observation is supported by phase noise characterization, frequency-resolved optical gating (FROG) pulse measurement, and numerical modeling [24,25]. The phase retrieval from the FROG measurement reveals a pulse structure akin to a cavity soliton: a 74 fs mode-locked pulse sitting on a cw background. Numerical modeling of the cw-driven nonlinear microresonator, capturing the full spectra with the measured GVD and *Q*s, confirms the feasibility of mode-locked pulse generation and agrees

with our measurements. We demonstrate, both experimentally and numerically, the importance of pump detuning and wavelength-dependent *Q*-factors in stabilizing and shaping the pulses generated from the normal GVD microresonators. Finally, we obtain the closed-form solution of the master equation under appropriate approximations, showing explicitly the connection between the microresonator parameters and the mode-locked pulse properties.

Figure 1a is the transmission of our Si_3N_4 microring resonator. Five modal families (3 TE and 2 TM) are identified from the transmission and each Lorentzian resonance is fitted to determine its frequency and *Q*-factor [26]. The frequency data is then used to evaluate the GVD. For the fundamental mode family, a loaded *Q*-factor of more than 10^6 is achieved at 1600 nm while the *Q*-factors at the telecommunications C-band wavelengths are more than 4× lower due to residual N-H absorption [27]. For the higher order mode families, *Q*-factors are orders of magnitude smaller and thus no Kerr comb is generated from these mode families. *Q*-factors are also reduced at longer than 1625 nm due to increasing coupling loss. Therefore, the resonator has a distinct spectrally restricted area characterized with the highest *Q*-factor. As discussed later, this feature is critical for the mode-locked pulse generation in our normal GVD microresonators. Figure 1b shows the measured fundamental mode dispersion of our ring resonator, in a good agreement with our numerical modeling using a full-vectorial finite-element mode solver. Across the whole L-band, the fundamental mode features a normal GVD with local disruptions induced by mode interaction with the higher-order modes. Such change of local GVD facilitates the start of the hyper-parametric oscillation from our microresonator [26]. An example Kerr comb spectrum is shown in Figure

1c, with a spectral width spanning more than 200 nm.

The optical spectrum shows a clean mode structure with comb lines separated by single free spectral range (FSR) of the fundamental mode family, without identifiable noise peaks between comb lines (Figure 1d, inset). We investigated the Kerr comb coherence by measuring the RF amplitude noise with a scan range much larger than the cavity linewidth and by performing a cw heterodyne beat note measurement [28,29]. Both measurements confirmed the coherence of the Kerr comb. The use of RF amplitude noise as a measure of low phase noise operation has been demonstrated and widely employed [13,28,29]. With proper change of the pump power and detuning, the Kerr comb is driven into the low phase noise regime as shown in Figure 1d. The cw heterodyne beat note measurements are shown in Figure 1e. Besides the beat note of the cw laser with the pump laser, beat notes between the cw laser and different comb lines are also measured. All beat notes exhibit the same linewidth of 800 kHz, limited by coherence between the cw laser and the pump laser. Neither additional linewidth broadening of the comb lines relative to the pump nor multiple beat notes were observed, confirming the comb lines exhibit a similar level of phase noise as the pump.

We measured the pulse duration via sub-femto-joule sensitive second-harmonic-generation (SHG) non-collinear frequency-resolved optical gating (FROG) [30,31] without involvement of any optical amplification nor external bandpass filtering, to minimize pulse distortion. Careful checks were conducted to ensure no interferometric SH signal was collected in the FROG spectrogram [32]. Figure 2a is the spectrogram with 32 ps delay scan and it shows a pulse train with 8.7 ps period, the inverse of the fundamental mode family FSR (115.56 GHz). For better visualization, Fig. 2a is plotted

on log-scale and the bright cw pump component is removed in the plot. Spectral interferometric fringes are clearly visible for delays longer than the pulse duration. This interference arises due to the presence of the cw background as it can also mix with the pulse, generating two temporally-separated FROG signal pulses. The fringes become sparse as the delay approaches zero and the patterns depend on the relative phase between the cw pump and the pulse [33]. Figure 2b and 2c is the spectrogram measured with a finer time resolution, 4 fs, and Figure 2c is the reconstructed spectrogram with a FROG error of 2.7%. Due to the complexity of the pulses, an iterative genetic algorithm is developed specifically to retrieve the spectrograms [26]. Figure 2d shows the retrieved pulse shape (red curve) and temporal phase profile (blue curve), with a 1.3 rad relative phase contrast observed within the pulse. The full-width-half-maximum (FWHM) pulse duration is measured at 74 fs, positively chirped from its transform-limited FWHM pulse duration of 55 fs. Due to the nature of the cw driven nonlinearity, the observed mode-locked pulse necessarily sits on a pedestal, analogous to a cavity soliton.

Figure 2e shows the measured optical intensity autocorrelation (AC) trace of the generated pulse train and the left panel of Figure 2f plots the zoom-in view. Of note, this is not an interferometric autocorrelation and thus the temporal fringes in the AC trace represent the actual oscillating structures of the pulse. Between the pulses, temporal fringes with a period of ~200 fs are clearly observed and these fringes arise from the presence of the primary comb lines, ~4.85 THz (42nd mode) away from the pump [26]. In addition, the right panel of Figure 2f shows the calculated AC traces of a stable transform-limited pulse train (black curve) and an unstable pulse train (red curve). As the instability results in the

significantly increased background level of the AC trace, it shows that the instability of the generated pulse train is minimal and provides another confirmation of the stable mode-locked pulse generation [34].

To shed light on the pulse generation mechanism, we first performed numerical simulation solving the Lugiato-Lefever equation for 512 modes around the cw pump [25]. Experimentally-measured dispersion (Figure 1b) and wavelength-dependent Q values (Figure S2), including the local dispersion disruptions, are entered into the modeling [26]. Figure 3a shows the simulation results, illustrating the emergence of the first pairs of hyper-parametric oscillation sidebands around the ±42nd modes. A good agreement with the experimental emergence result (inset) is achieved. With the proper pump power and detuning, a fundamentally mode-locked pulse train is generated as shown in Figure 3b. The modeled FWHM pulse duration is 110 fs and the relative phase contrast is 1.7 rad (positively chirped), in good agreements with the FROG measurements.

We next numerically examined idealistic nonlinear microresonators characterized by solely normal GVDs and symmetric wavelength-dependent Q factors to elucidate the mode-locking physics [26]. Figure S14 shows the case with larger D_2 of 0.03 (or -2.7 MHz) and without wavelength dependence in Q factors. A phase-locked Kerr comb can be generated, but the pulse duration is long and the shape complex. This is because, unlike in anomalous GVD microresonators, pulse broadening due to the normal GVD is not balanced by SPM and thus an additional mechanism has to be introduced to stabilize and shape the pulses. In Figure S15, we numerically introduce wavelength-dependent Q-factors, effectively a bandpass filter, and then clean mode-locked pulses are generated from the microresonator.

These are dark pulses and the exact pulse shapes depend on the bandpass filter bandwidth. Next, when D_2 is numerically set smaller at 0.003 (and closer to the experimental value), bright pulses can also be observed. Different from the case of large normal dispersion where only dark pulses exist, both bright and dark pulses are possible in the small normal dispersion case, depending on the exact combination of dispersion and bandpass filter bandwidth (Figure S16). It is even possible to generate square pulses directly with the correct sets of *Q*-factor profile, GVD, and detuning (Figure 3c). We note that the mode-locking mechanism has analogies, but is not identical, to the pulse generation mechanism in all-normal dispersion fiber lasers [35], a variant of additive pulse mode-locking [36].

To experimentally examine the effect of wavelength-dependent *Q*-factors, we then re-annealed the same microresonator at 1200°C to reduce the absorption in the shorter wavelengths such that the *Q* roll-off is less pronounced (Figure S2). Figure 4a shows the Kerr comb generated from the re-annealed microresonator, showing a smoother and broader spectrum than the one shown in Figure 1c. Similarly, the comb can be driven into a low phase noise state (Figure 4b). However, now without the effective narrow bandpass filter, mode-locked pulses are not observed as evidenced by the high background level (≈ 0.85) in the AC trace. A phase stable state without mode-locking is also observed in another recent study using a different microresonator platform [37].

Furthermore, we seek the closed-form solution of the master equation for the Kerr comb and pulse generation:

$$T_R \frac{\partial}{\partial T} A + \frac{i}{2}\left(\beta_{2\Sigma} + i\frac{T_c}{\Omega_f^2}\right)\frac{\partial^2}{\partial t^2} A - i\gamma|A|^2 A = -\left(\alpha + \frac{T_c}{2} + i\delta_0\right) A + i\sqrt{T_c P_{in}} e^{i\varphi_{in}} \qquad (1)$$

where $A(T, t)$ is the microresonator electric field slowly-varying envelope, T_R the cavity

roundtrip time, t the retarded time, T the slow time of the cavity, $\beta_{2\Sigma}$ the cavity GVD, T_c the power coupling loss per roundtrip, Ω_f the spectral characteristics of the coupling, γ the nonlinear coefficient, α the amplitude attenuation per roundtrip, δ_0 the resonance detuning, and $\sqrt{P_{in}}e^{i\varphi_{in}}$ the cw pump. Here, for simplicity, we assume the intracavity bandpass filter results solely from wavelength-dependent coupling loss: $T_{coupling} \approx T_c\left[1+\frac{(\omega_c-\omega)^2}{\Omega_f^2}\right]$, where ω_c is the frequency for maximal coupling. Assuming Gaussian input pulse and applying the variational method, the equations describing the mode-locked pulses are derived in equations (S9) [26]. Defining chirp q, pulse energy E_p, and the pulse duration τ, and with $q^2 \gg \Omega_f^2\tau^2 \gg 1$, we obtain the resulting solutions:

$$E_p \approx \frac{8\sqrt{10\pi}}{15}\frac{\beta_{2\Sigma}^{3/2}\Omega_f^2\sqrt{\delta_0}}{T_c\gamma} \tag{2}$$

$$\tau \approx \frac{2\sqrt{5}}{3}\frac{\beta_{2\Sigma}^{3/2}\Omega_f^2}{T_c\sqrt{\delta_0}} \tag{3}$$

$$q \approx \frac{4\beta_{2\Sigma}\Omega_f^2}{3T_C} \tag{4}$$

By fitting the measured Q-factor (Figure S2) of the ±20 modes around Q_{max} with the wavelength-dependent coupling loss profile defined above, a filter bandwidth of 2.3 THz is found. A chirp q of 1.6 is then obtained after the filter bandwidth and the other measured parameters ($T_c = 0.003, \beta_{2\Sigma} = 17.14\ fs^2$) are entered into equation (4). This chirp is close to that obtained from the FROG measurement ($q = 1.5$), and the resulting calculated FWHM pulse duration (98 fs) is close to our measurements.

While the total power in the microresonator reduces as the pump detuning gets larger, equations (2) and (3) show the pulse energy actually increases and the pulse duration gets shorter. Overall, the pulse quality improves. It illustrates the active role of pump detuning: it

is not simply a parameter that controls the coupled power in the microresonator, but an important physical factor that determines the pulse duration and energy distribution between the pulse and cw background. Furthermore, the closed-form solutions show that the pulse generated from a normal GVD microresonator is always chirped [equation (4)], and a narrower bandpass filter is necessary to keep the pulse short when the dispersion increases.

In summary we present the generation of mode-locked pulses from on-chip normal dispersion microresonator, supported by phase noise characterization, FROG pulse measurement, and numerical modeling with exact experimental parameters. The excitation of the hyper-parametric oscillation is facilitated by the local dispersion disruptions induced by mode interactions. Then the system is driven from the hyper-parametric oscillation to the mode-locked pulse generation by a proper change of the pump power and detuning. The phase retrieval from the FROG measurement reveals a 74 fs fundamentally mode-locked pulse sitting on a cw background. Numerical modeling of the cw-driven nonlinear microresonator, capturing the full spectra with the measured GVD and *Q*s, confirms the feasibility of mode-locked pulse generation and agrees with our measurements. We show, both experimentally and numerically, the importance of pump detuning and effective bandpass filtering in stabilizing and shaping the pulses generated from normal GVD microresonators. Finally, we present the closed-form solution of the master equation under appropriate approximations, facilitating the design of mode-locked pulse generation from microresonators.

Acknowledgements:

The authors acknowledge discussions with Erich P. Ippen, Zhenda Xie, and Jiangjun Zheng, a

spectroscopic ellipsometer measurement and analysis at Brookhaven National Laboratory by Felice Gesuele and Tingyi Gu, respectively, and loan of the L-band EDFA and the RF spectrum analyzer from the Bergman and Shepard groups at Columbia respectively.

*swhuang@seas.ucla.edu

†cheewei.wong@ucla.edu

References:

[1] P. Del'Haye, A. Schliesser, O. Arcizet, T. Wilken, R. Holzwarth, and T. J. Kippenberg, *Nature* **450**, 1214 (2007).

[2] A. A. Savchenkov, A. B. Matsko, V. S. Ilchenko, I. Solomatine, D. Seidel, and L. Maleki, *Phys. Rev. Lett.* **101**, 093902 (2008).

[3] P. Del'Haye, O. Arcizet, A. Schliesser, R. Holzwarth, and T. J. Kippenberg, *Phys. Rev. Lett.* **101**, 053903 (2008).

[4] J. S. Levy, A. Gondarenko, M. A. Foster, A. C. Turner-Foster, A. L. Gaeta, and M. Lipson, *Nat. Photon.* **4**, 37 (2010).

[5] L. Razzari, D. Duchesne, M. Ferrera, R. Morandotti, S. Chu, B. E. Little, and D. J. Moss, *Nat. Photon.* **4**, 41 (2010).

[6] Y. Okawachi, K. Saha, J. S. Levy, Y. H. Wen, M. Lipson, and A. L. Gaeta, *Opt. Lett.* **36**, 3398 (2011).

[7] T. J. Kippenberg, R. Holzwarth, and S. A. Diddams, *Science* **332**, 555 (2011).

[8] F. Ferdous, H. Miao, D. E. Leaird, K. Srinivasan, J. Wang, L. Chen, L. T. Varghese, and A. M. Weiner, *Nat. Photon.* **5**, 770 (2011).

[9] M. A. Foster, J. S. Levy, O. Kuzucu, K. Saha, M. Lipson, and A. L. Gaeta, *Opt. Express* **19**, 14233 (2011).

[10] M. Peccianti, A. Pasquazi, Y. Park, B. E. Little, S. T. Chu, D. J. Moss, and R. Morandotti, *Nat. Commun.* **3**, 765 (2012).

[11] F. Ferdous, H. Miao, P.-H. Wang, D. E. Leaird, K. Srinivasan, L. Chen, V. Aksyuk, and A. M. Weiner, *Opt. Express* **20**, 21033 (2012).

[12] T. Herr, V. Brasch, J. D. Jost, C. Y. Wang, N. M. Kondratiev, M. L. Gorodetsky, and T. J. Kippenberg, *Nat. Photon.* **8**, 145 (2014).

[13] K. Saha, Y. Okawachi, B. Shim, J. S. Levy, R. Salem, A. R. Johnson, M. A. Foster, M. R. E. Lamont, M. Lipson, and A. L. Gaeta, *Opt. Express* **21**, 1335 (2013).

[14] D. J. Moss, R. Morandotti, A. L. Gaeta, and M. Lipson, *Nat. Photon.* **7**, 597 (2013).

[15] J. Riemensberger, K. Hartinger, T. Herr, V. Brasch, R. Holzwarth, and T. J. Kippenberg, *Opt. Express* **20**, 27661 (2012).

[16] V. S. Ilchenko, A. A. Savchenkov, A. B. Matsko, and L. Maleki, *J. Opt. Soc. Am. A* **20**,

157 (2003).
[17] C. J. Chen, C. A. Husko, I. Meric, K. L. Shepard, C. W. Wong, W. M. J. Green, Y. A. Vlasov, and S. Assefa, *Appl. Phys. Lett.* **96**, 081107 (2010).
[18] L. Zhang, C. Bao, V. Singh, J. Mu, C. Yang, A. M. Agarwal, L. C. Kimerling, and J. Michel, *Opt. Lett.* **38**, 5122 (2013).
[19] A. B. Matsko, A. A. Savchenkov, and L. Maleki, *Opt. Lett.* **37**, 43 (2012).
[20] T. Hansson, D. Modotto, and S. Wabnitz, *Phys. Rev. A* **88**, 023819 (2013).
[21] C. Godey, I. V. Balakireva, A. Coillet, and Y. K. Chembo, *Phys. Rev. A* **89**, 063814 (2014).
[22] A. Coillet, I. Balakireva, R. Henriet, K. Saleh, L. Larger, J. M. Dudley, C. R. Menyuk, and Y. K. Chembo, *IEEE Photon. J.* **5**, 6100409 (2013).
[23] I. S. Grudinin, L. Baumgartel, and N. Yu, *Opt. Express* **21**, 26929 (2013).
[24] Y. K. Chembo and N. Yu, *Phys. Rev. A* **82**, 033801 (2010).
[25] S. Coen, H. G. Randle, T. Sylvestre, and M. Erkintalo, *Opt. Lett.* **38**, 37 (2013).
[26] Supplementary Information.
[27] R. Germann, H. W. M. Salemink, R. Beyeler, G. L. Bona, F. Horst, I. Massarek, and B. J. Offrein, *J. Electrochem. Soc.* **147**, 2237 (2000).
[28] T. Herr, K. Hartinger, J. Riemensberger, C. Y. Wang, E. Gavartin, R. Holzwarth, M. L. Gorodetsky, and T. J. Kippenberg, *Nat. Photon.* **6**, 480 (2012).
[29] C. Y. Wang, T. Herr, P. Del'Haye, A. Schliesser, J. Hofer, R. Holzwarth, T. W. Hänsch, N. Picqué, and T. J. Kippenberg, *Nat. Commun.* **4**, 1345 (2013).
[30] R. Trebino, *Frequency-Resolved Optical Gating: The Measurement of Ultrashort Laser Pulses* (Springer, 2000).
[31] C. A. Husko, S. Combrié, P. Colman, J. Zheng, A. D. Rossi, and C. W. Wong, *Sci. Rep.* **3**, (2013).
[32] G. Stibenz and G. Steinmeyer, *Opt. Express* **13**, 2617 (2005).
[33] J. K. Jang, M. Erkintalo, S. G. Murdoch, and S. Coen, *Nat. Photon.* **7**, 657 (2013).
[34] M. Rhodes, G. Steinmeyer, J. Ratner, and R. Trebino, *Laser Photon. Rev.* **7**, 557 (2013).
[35] A. Chong, W. H. Renninger, and F. W. Wise, *J. Opt. Soc. Am. B* **25**, 140 (2008).
[36] H. A. Haus, J. G. Fujimoto, and E. P. Ippen, *J. Opt. Soc. Am. B* **8**, 2068 (1991).
[37] P. Del'Haye, K. Beha, S. B. Papp, and S. A. Diddams, *Phys. Rev. Lett.* **112**, 043905 (2014).
[38] See Supplemental Material [url], which includes Refs. [39-53].
[39] J. Riemensberger, K. Hartinger, T. Herr, V. Brasch, R. Holzwarth, and T. J. Kippenberg, *Opt. Express* **20**, 27661 (2012).
[40] S. L. Gilbert, W. C. Swann, and C. M. Wang, *Natl. Inst. Stnd. Technol. Spec. Publ.* **260**, 137 (1998).
[41] P. Del'Haye, O. Arcizet, M. L. Gorodetsky, R. Holzwarth, and T. J. Kippenberg, *Nat. Photon.* **3**, 529 (2009).
[42] A. Arbabi and L. L. Goddard, *Opt. Lett.* **38**, 3878 (2013).
[43] C.-L. Tien and T.-W. Lin, *Appl. Opt.* **51**, 7229 (2012).
[44] A. A. Savchenkov, A. B. Matsko, W. Liang, V. S. Ilchenko, D. Seidel, and L. Maleki, *Opt. Express* **20**, 27290 (2012).
[45] T. Herr, V. Brasch, J. D. Jost, I. Mirgorodskiy, G. Lihachev, M. L. Gorodetsky, and T. J.

Kippenberg, *Phys. Rev. Lett.* **113**, 123901 (2014).
[46] A. B. Matsko, W. Liang, A. A. Savchenkov, and L. Maleki, *Opt. Lett.* **38**, 525 (2013).
[47] F. C. Cruz, J. D. Marconi, A. Cerqueira S. Jr., and H. L. Fragnito, *Opt. Commun.* **283**, 1459 (2010).
[48] L. E. Nelson, S. B. Fleischer, G. Lenz, and E. P. Ippen, *Opt. Lett.* **21**, 1759 (1996).
[49] J. W. Nicholson, F. G. Omenetto, D. J. Funk, and A. J. Taylor, *Opt. Lett.* **24**, 490 (1999).
[50] D. E. Goldberg, *Genetic Algorithms in Search, Optimization, and Machine Learning* (Addison-Wesley, 1988).
[51] A. A. Savchenkov, W. Liang, A. B. Matsko, V. S. Ilchenko, D. Seidel, and L. Maleki, *Opt. Lett.* **34**, 1318 (2009).
[52] X. Xue, Y. Xuan, Y. Liu, P.-H. Wang, S. Chen, J. Wang, D. E. Leaird, M. Qi, and A. M. Weiner, arXiv:1406.1116 (2014).
[53] A. Hasegawa, *IEEE J. Sel. Top. Quant. Electron.* **6**, 1161 (2000).

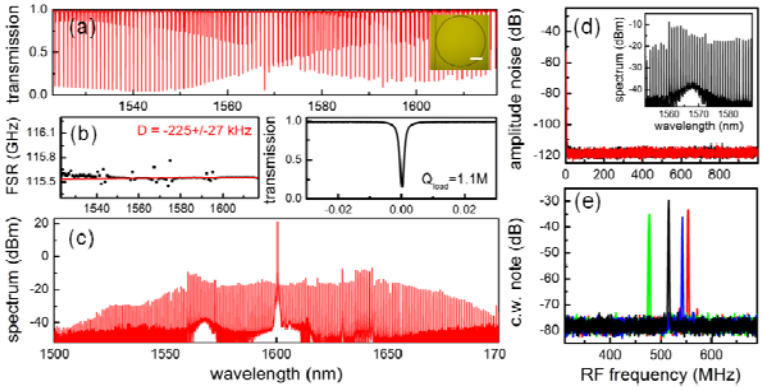

FIG. 1 (a) Transmission of the cavity modes. Inset: an optical micrograph of the ring resonator. Scale bar: 100μm. (b) Left: wavelength dependent FSR, measuring a non-equidistance of the modes, , of -225kHz, in a good agreement with the simulation result from a full-vector finite-element mode solver, . Right: transmission of the cavity mode at the pump wavelength, measuring a quality factor of . (c) Example Kerr comb spectrum, with a spectral width spanning more than 200 nm. (d) RF amplitude noise of the Kerr comb (black curve) along with the detector background (red curve), indicating the low phase noise operation. Inset: a zoom-in plot of the optical spectrum, showing a clean comb structure. (e) cw heterodyne beat notes between a cw laser and different comb lines (black: pump; blue: 10th mode; red: 20th mode; green: 21st mode). No linewidth broadening of the comb lines relative to the pump is observed, showing the comb retains a similar level of phase noise as the cw laser.

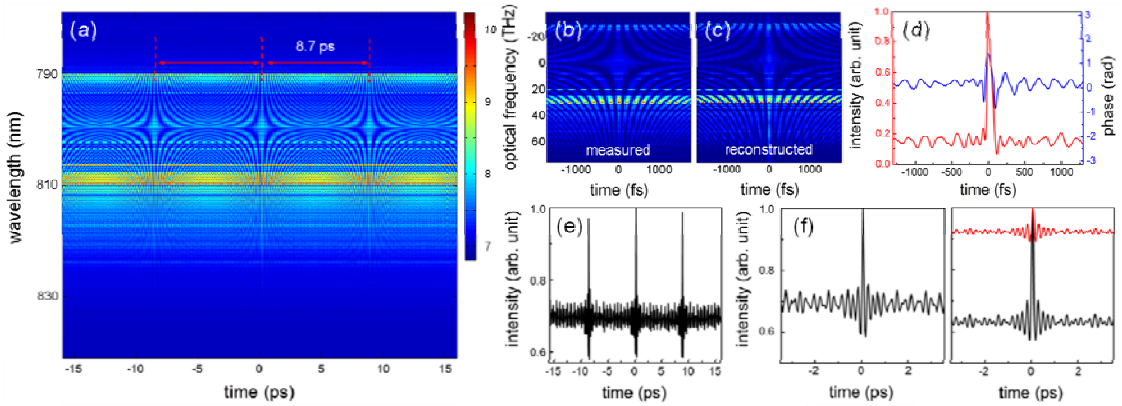

FIG. 2 (a) FROG spectrogram with a delay scan of 32 ps, showing a fundamentally mode-locked pulse train. (b) FROG spectrogram measured with a finer time resolution of 4 fs. (c) Reconstructed FROG spectrogram achieved by use of genetic algorithms. (d) Retrieved pulse shape (red curve) and temporal phase profile (blue curve), measuring a 74 fs FWHM pulse duration. (e) Measured AC of the generated fundamentally mode-locked pulse train. (f) Left: a zoom-in plot of the measured AC. Right: the calculated ACs of a transform-limited stable pulse train (black curve) and an unstable pulse train showing a significantly larger AC background (red curve).

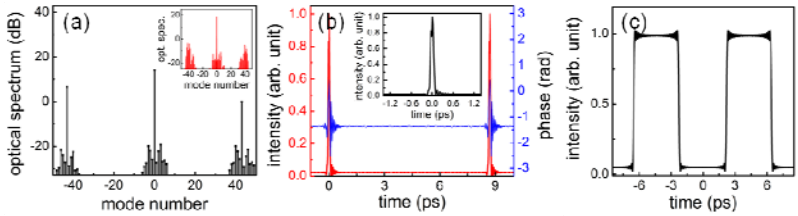

FIG. 3 (a) Near the threshold and with a small red-detuning of 180 MHz, the first pairs of hyper-parametric oscillation sidebands emerge at around the ± 42nd modes, showing a good agreement with the experimental result (inset). (b) With the proper pump power (260 mW) and red-detuning (2.5 GHz), a mode-locked pulse train is generated. The red and blue curves are the modeled pulse shape and the temporal phase profile, respectively. Inset: a zoom-in plot of the pulse shape, showing an ultrashort FWHM pulse duration of 110 fs. (c) Square optical pulses can also be generated directly from a normal GVD microresonator. The conditions for the observation of these square pulses are , red-detuning of , resonance linewidth of and pump power 25 times larger than the threshold.

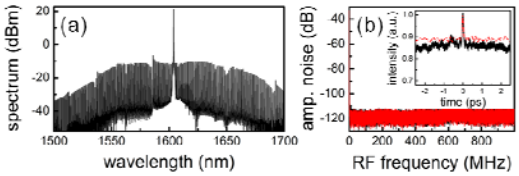

FIG. 4 (a) Example Kerr comb spectrum from the re-annealed microresonator, showing a smoother and broader spectrum. (b) RF amplitude noise of the Kerr comb (black curve) along with the detector background (red curve). While the Kerr comb can also be driven to a low phase noise state, the high background level of the AC trace (inset) indicates the absence of mode-locked pulses. The red dashed line is the calculated AC trace assuming random spectral phases.